Low Frequency Current Density Imaging Cylindrical Phantom Experiment

Tim DeMonte
June 14, 2001

Contents:

Purpose:

The purpose of this experiment is to demonstrate the Low Frequency Current Density Imaging (LF-CDI) technique in a simple cylindrical phantom. The results of this experiment should show that current flows in one direction and is uniformly distributed throughout the cylinder. This experiment is a good starting point for researchers who are interested in developing their own LF-CDI system. It is a simple experiment that demonstrates most of the important principles involved in LF-CDI.

Description of Cylindrical Phantom:

The cylindrical phantom is shown in Figure 1. This cylinder is constructed of plexiglas (i.e. acrylic) and has a diameter of 152 mm and a height of 267 mm (inside dimensions), although a smaller cylinder may also be used. The solution inside the phantom consists of distilled water, 0.9g/100 mL NaCl and 0.064g/100 mL $CuSO_4$. The NaCl increases the conductivity of the solution and the $CuSO_4$ provides reasonable T_1 and T_2 relaxation constants (approx. T_1 = 200 ms and T_2 = 170 ms). Copper disk electrodes cover the top and bottom of the cylinder. Current is applied to the phantom through the feed wires shown in Figure 1.

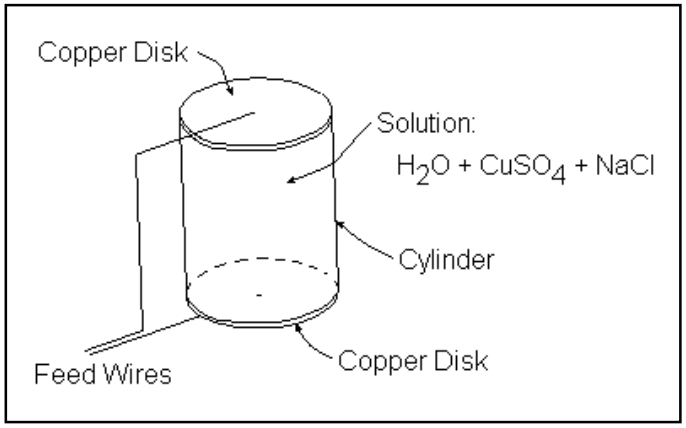

Figure 1: Cylindrical phantom with copper disks on top and bottom and a feed wire connected to each disk.

Theoretical Background:

The phantom coordinate system is given in Figure 2. The LF-CDI technique measures B_x and B_y such that J_z can be computed from Ampere's Law

$$\mathbf{J} = \nabla \times \mathbf{H} \tag{1}$$

which can be partially expanded in cartesian coordinates as

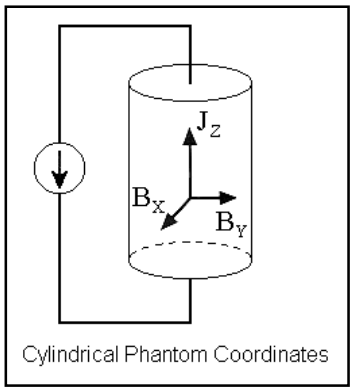

Figure 2: Coordinate system defined for phantom frame of reference showing two orthogonal components of magnetic field to be measured.

$$J_z = \frac{1}{\mu_0}\left[\frac{\partial B_y}{\partial x} - \frac{\partial B_x}{\partial y}\right] \tag{2}$$

Components of the **B** field produced by the externally applied current are encoded in the MR phase images. The phase angle, Γ, produced by a current induced magnetic field component, B_J, which is parallel to the B_0 field, is given by

$$\Gamma = \gamma B_J T_c \tag{3}$$

where T_c is the duration of the applied current pulse and γ is the gyromagnetic ratio. Equation (3) shows a linear relationship between the information encoded in a phase image and the magnetic field component parallel to the B_0 field of the MRI system. Equation (2) shows that two orthogonal components of magnetic field must be measured to compute one component of current density.

Pulse Sequence:

A spin echo sequence is normally used for LF-CDI due to its high signal to noise ratio (SNR), although other sequences may be used. Figure 3 shows a typical spin echo sequence with the required current pulses used for LF-CDI. A DC current is applied to the phantom between the 90° RF pulse and the 180° RF pulse and is also applied between the 180° RF pulse and the readout gradient. The second pulse has opposite polarity to the first pulse because the spin systems are reversed after the 180° RF pulse. The timing of these current pulses is adjusted to avoid overlapping any of the RF pulses.

Phase cycling is used to remove any systematic errors that arise from constant phase terms. To accomplish this phase cycling, two acquisitions are performed with opposite current polarity applied on each acquisition. During data processing, these two acquisitions are subtracted and divided by 2 such that the constant phase terms cancel out and the signal is increased by the averaging of the two acquisitions just as in NEX=2 pulse sequences. Figure 4 shows an example of a spin echo pulse sequence that

demonstrates current pulses and phase cycling for 256 phase encode steps and 5 slices (gradients are not shown).

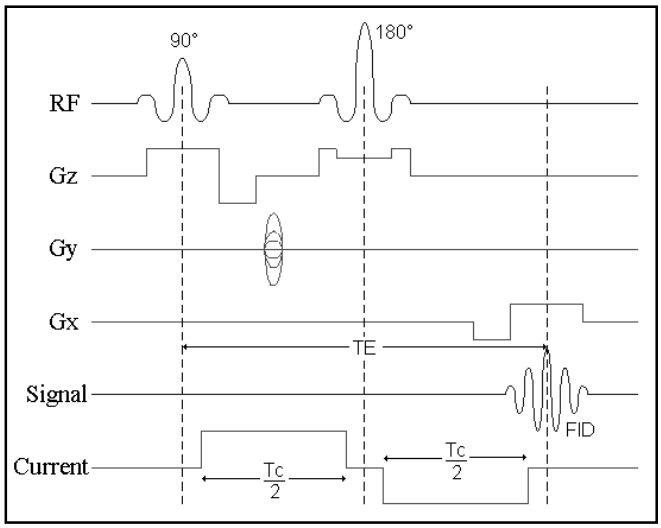

Figure 3: The spin echo pulse sequence for LF-CDI. A square current pulse is applied between the 90° and 180° RF pulses. An equal and opposite polarity pulse is applied following the 180° RF pulse.

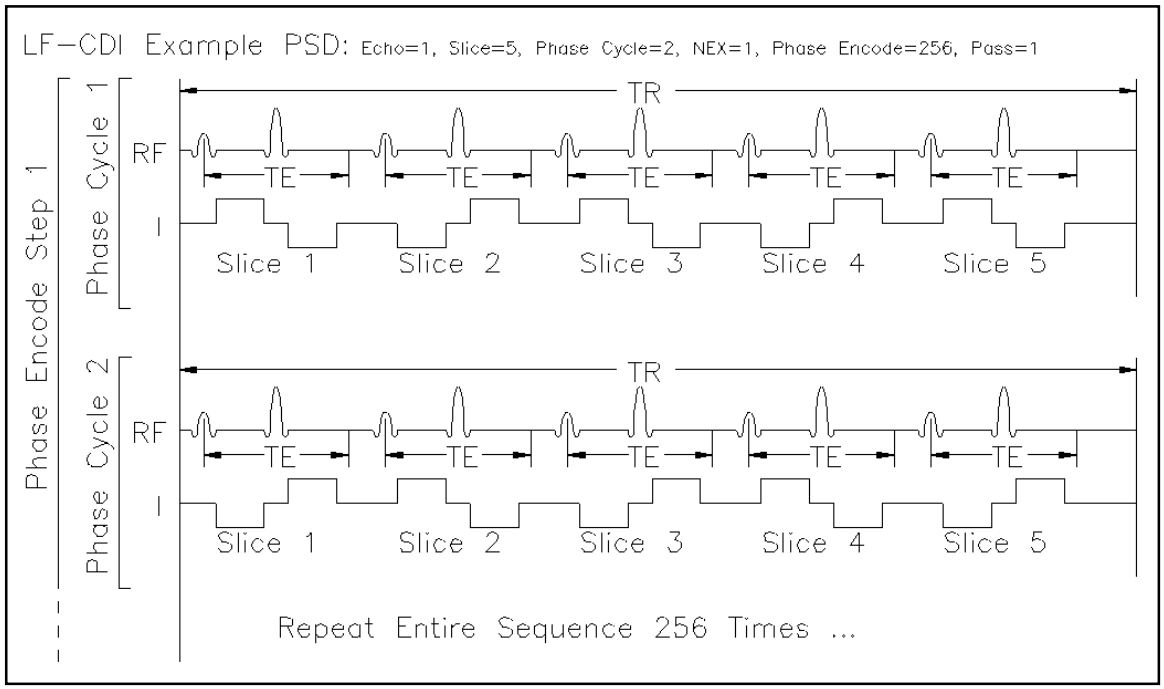

Figure 4: An example of a complete LF-CDI sequence showing the RF pulses and current pulses (gradient pulses not shown). In this sequence, 5 slices are acquired in the first phase cycle followed by an acquisition of the same 5 slices for the second phase cycle. The current polarity is reversed during the second phase cycle. The entire sequence shown in the diagram is repeated for each phase encoding step (i.e. 256 times).

Experimental Method:

In this experiment, the cylinder is placed in an upright position as shown in Figure 5. A coronal slice plane is taken through the center of the cylinder (multi-slices may be acquired). The two orientations corresponding to the independent measurements of B_y and B_x and are shown in Figures 5 (a) and 5 (b), respectively.

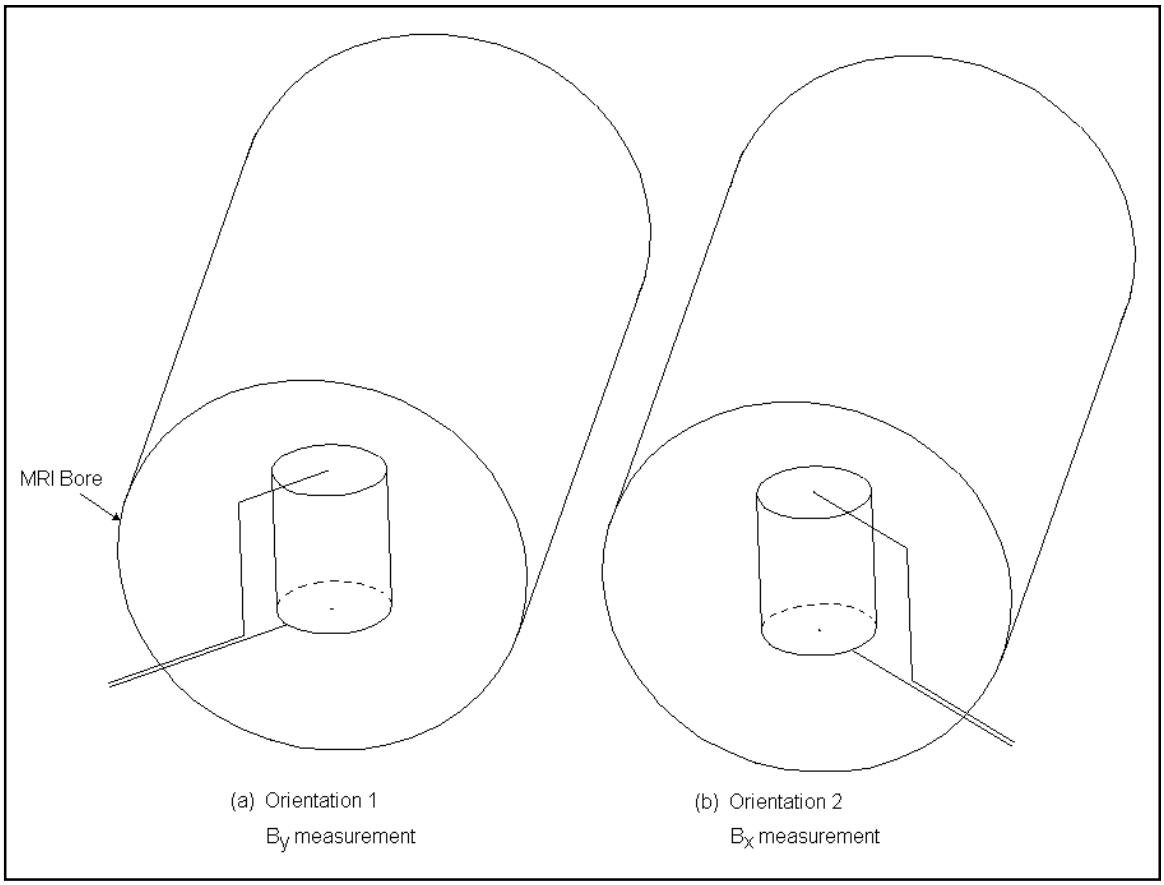

Figure 5: The two orthogonal orientations of the cylinder phantom in the MRI system bore. (a) Orientation 1 – measurement of B_y. (b) Orientation 2 – measurement of B_x. Coronal slice planes are acquired through the center of the cylinder.

Typical MRI and CDI system parameters are given in Table 1. T_c is typically a few milliseconds shorter than TE (i.e. 5 ms for this experiment) as can be seen in Figure 3.

Table 1: MRI and CDI Parameters Used in Cylindrical Phantom Experiment

Parameter	Value
B_0	1.5 T
Pulse Sequence	Spin Echo
TR	700 ms
TE	93 ms
T_c	88 ms
Current Amplitude	50 mA
Frequency Encode Steps	256
Phase Encode Steps	256
Field of View	320 x 320 mm
Slice Thickness	1.2 mm
Slice Gap	0 mm
Number of Slices	5
Coil Type (Tx/Rx)	Body

Either orientation may be acquired first, although the data processing program described in Figure 6 requires the B_y orientation first and the B_x orientation second. It is recommended that the current pulses be turned off during the prescan sequences.

Data Processing:

The data processing steps essentially compute one component of current density from the two separate component measurements of magnetic field as indicated in Equation (2). The actual steps of this computation are shown in Figure 6. Beginning with complex k-space data, the FFT is performed and both the magnitude and phase of the data are obtained for the first phase cycle of each orientation. For each of the second phase cycles, only the phase is obtained. The image data must now be aligned between the two orientations. The first step in alignment is to rotate the second orientation data by 90° to match the first orientation data. Additionally, a translation will be required to further align the two image sets.

The two magnitude images are used to generate binary mask images where '1' indicates a pixel of high signal and '0' indicates a pixel of low signal. The threshold value for deciding between low and high signal is obtained by

$$Threshold = \frac{2\mu}{\sqrt{\pi}}(factor) \qquad (4)$$

where $\frac{2\mu}{\sqrt{\pi}}$ is an estimate of the standard deviation in the data and μ is the mean value of a region of noisy, 'zero' signal pixels in the magnitude image. In Equation (4), *factor* is

assigned an arbitrary value that is used to adjust the threshold. Typical values range between 0.0 and 5.0 where 0.0 effectively turns off the thresholding and 5.0 is considered a high level of thresholding. For processing the cylinder data, a *factor* of 3.0 was used. Masking is performed on phase images by multiplying the binary masks and phase images together.

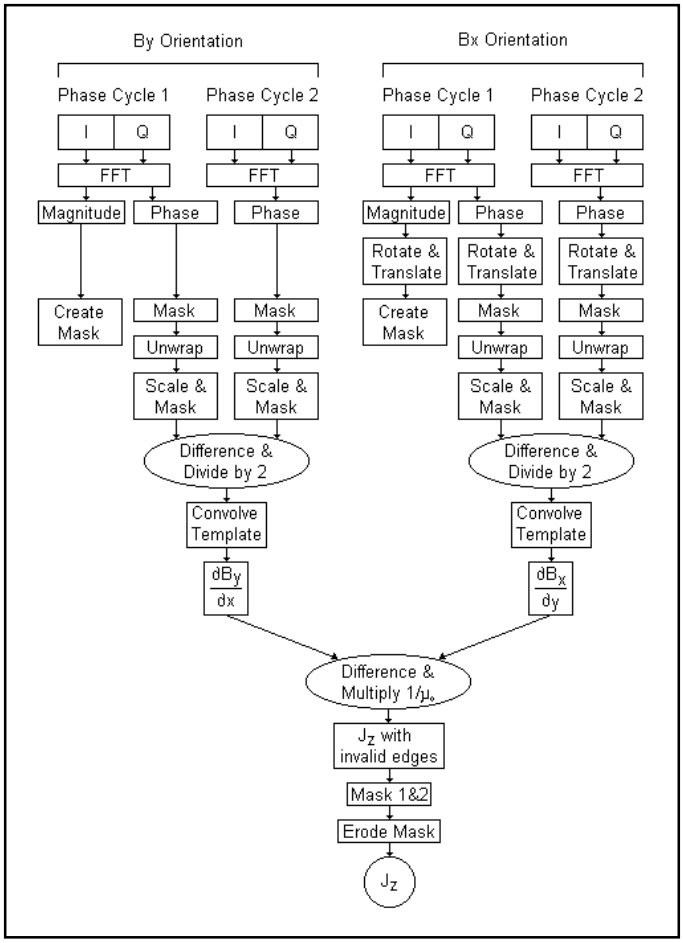

Figure 6: Data processing steps for a two-dimensional LF-CDI experiment. 'I' and 'Q' stand for 'In-phase' and 'Quadtrature' components of k-space, respectively.

Phase images from an MRI system are phase wrapped between the limits of $\pm\pi$. For example, the phase angles of –175° and +185° appear as the same value in a wrapped phase image. A phase unwrapping procedure must be applied to the phase images before further processing. Ideally, a two-dimensional phase unwrapping procedure can unwrap phase in all directions. However, a one-dimensional unwrapping (line-by-line) procedure will suffice provided that the direction of unwrapping corresponds to the direction of computing differences when the derivative templates (described later) are convolved with the phase images. Phase wrapping imposes a limit on any CDI experiment which is that the phase difference between any two adjacent pixels cannot exceed π or else they cannot be properly resolved in the unwrapping procedure.

After phase unwrapping, the data in the phase images is scaled from phase angles to magnetic fields according to Equation (3). Optionally, the images may be masked a second time to remove any streaks caused by the phase unwrapping. Next, the phase cycles are subtracted from each other and the resulting difference images are divided by 2.

Derivatives of the magnetic fields are estimated by convolving the following templates with the unwrapped difference images

$$\frac{1}{8\Delta x}\begin{bmatrix} -1 & 0 & 1 \\ -2 & 0 & 2 \\ -1 & 0 & 1 \end{bmatrix} \text{ for computing } \frac{\partial B_y}{\partial x} \tag{5a}$$

$$\frac{1}{8\Delta y}\begin{bmatrix} -1 & -2 & -1 \\ 0 & 0 & 0 \\ 1 & 2 & 1 \end{bmatrix} \text{ for computing } \frac{\partial B_x}{\partial y} \tag{5b}$$

where Δx and Δy are the pixel dimensions. The image coordinate system corresponding to these templates is given in Figure 7. As mentioned previously, the phase unwrapping must occur along the same dimension as the differencing. For example, phase unwrapping is performed along the x-axis for computing the derivative given in Equation (5a).

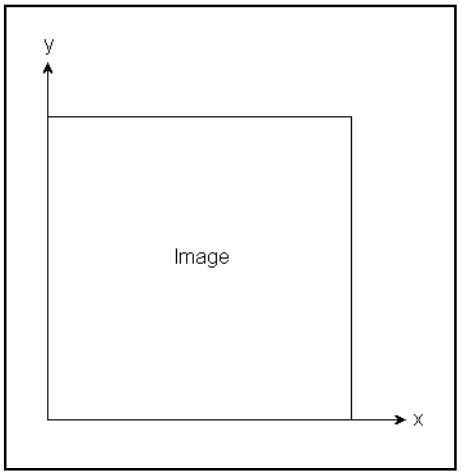

Figure 7: Image coordinates.

The two derivative images are subtracted according to Equation (2) and scaled by $1/\mu_0$ where μ_0 is the permeability of free space. The resulting image is one component of current density, J_z. The edges of objects containing high signal pixels in the image will not be computed correctly because the templates of Equations (5a) and (5b) use the 8 nearest neighbours to compute the derivative estimate for a given pixel. If some of these neighbouring pixels have been set to zero by the masking process, the resulting derivative estimate will be incorrect. An erosion process is applied to the combined mask to remove these invalid pixels from the current density image. The combined mask is a mask formed by an AND operation between the masks created from two orientations.

Results:

Some images from the cylinder experiment will be presented in this section as a guide to what should be expected. Figure 8 (a) shows a phase image of the cylinder. The object in the center of the phantom is a plastic rod. Phase noise is apparent outside of the cylinder producing random values in the range $\pm\pi$ radians. After masking the image, Figure 8 (b) shows the same phase image without the phase noise. Figure 8 (c) shows the same phase image after unwrapping along the x-axis and scaling according to Equation (3). The units of the color map are now in Tesla instead of radians. Also notice

the streaking artifact of the line-by-line phase unwrapping method. This artifact does not cause any problems with the final computation of current densities which are shown in Figure 8 (d).

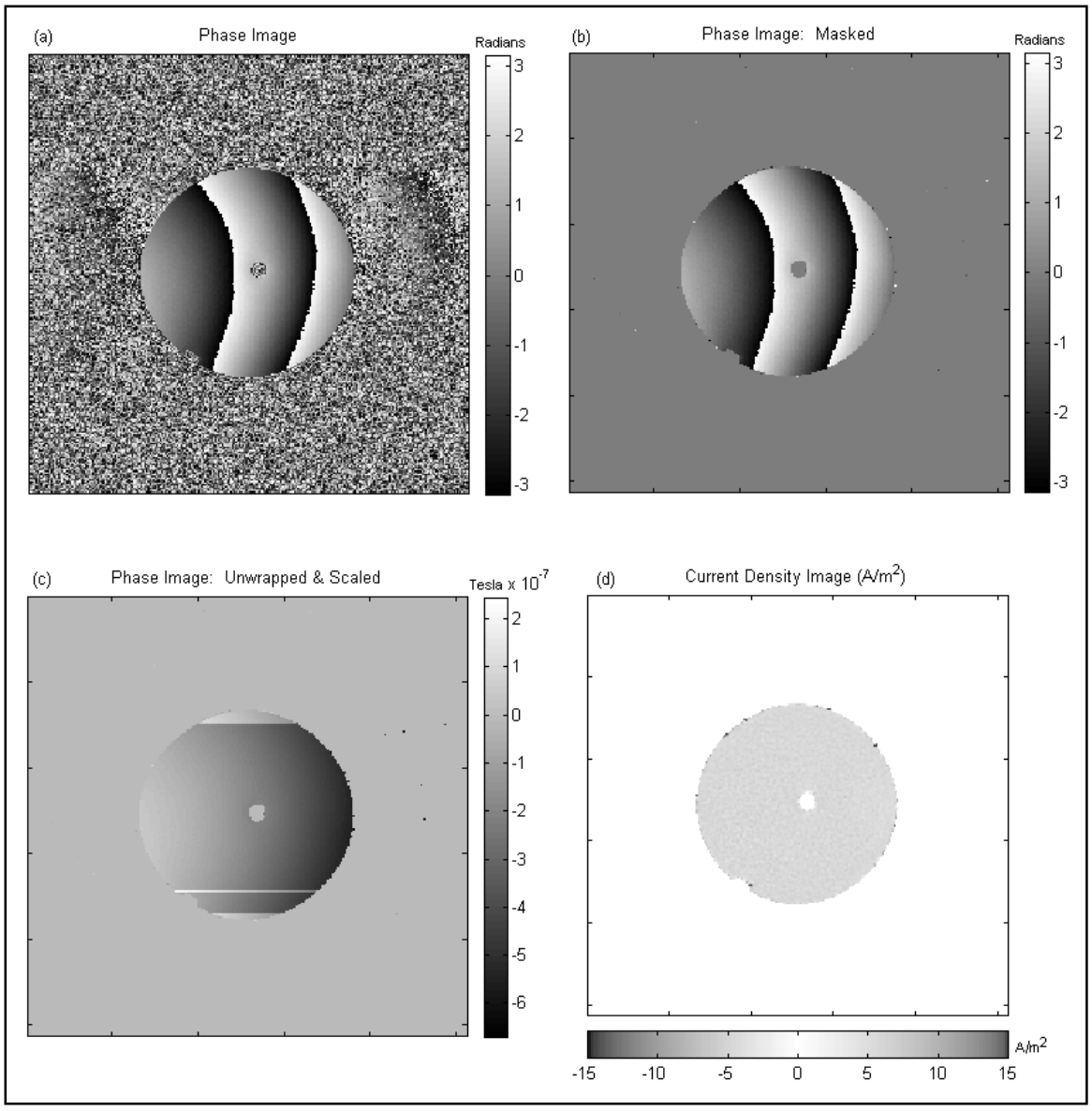

Figure 8: Some example images from the LF-CDI cylinder experiment. (a) Phase image. (b) The same phase image with the mask applied. (c) The same phase image after unwrapping and scaling. (d) The resulting current density image showing a uniform distribution across the cylinder's cross-section.

References:

[1] G. C. Scott, M. L. G. Joy, R. L. Armstrong, and R. M. Henkelman. Sensitivity of Magnetic Resonance Current Density Imaging. *J. Mag. Res.*, 97, pp. 235-254, 1992.

[2] G. C. Scott, M. L. G. Joy, R. L. Armstrong, and R. M. Henkelman. Measurement of nonuniform current density by magnetic resonance. *IEEE Transactions on Medical Imaging,* Vol. 10, No. 3, pp. 362-374, 1991.

[3] Greig Cameron Scott. *NMR Imaging of Current Density and Magnetic Fields*. PhD thesis, University of Toronto, 1993.

[4] Tim DeMonte. *Multi-slice Current Density Imaging: Implementation and Applications*. M.A.Sc. thesis, University of Toronto, 2001.